Title: Light scatter and fluorescence calibration allow standard comparisons of small particle data between different instruments.

Welsh J.A.[1*], Tang V.A.[2*]

[1]Translational Nanobiology Section, Laboratory of Pathology, Center for Cancer Research, National Cancer Institute, National Institutes of Health, Bethesda, Maryland, 20892, USA.

[2]University of Ottawa, Flow Cytometry and Virometry Core Facility

**corresponding authors: joshua.welsh@nih.gov, vtang@uottawa.ca*

Abstract

Flow cytometry analysis has been utilized since the late 1970s for the analysis of small particles, initially viruses before extracellular vesicles (EVs) in the 1990s. Despite its long-established use, a lack of standardization has resulted in a growing body of literature that is cannot be easily interpreted, validated, and reproduced between instrumentation. This inconsistency in data reporting greatly impacts the progress of the small particle field by making it difficult for researchers to make objective assessments on assays and instrumentation for small particle analysis. The methods and reagents for fluorescence and light scatter standardization are not novel. In this pilot study, we demonstrate calibration of small particle data with commercially available materials, published methods, and freely available software tools. We show that light scatter, fluorescence, and concentration can be calibrated and result in highly concordant data between flow cytometry platforms independent of instrument collection angle or gain/voltage; providing a means of cross-comparison in standard units.

Introduction

Efforts to standardize flow cytometry (FCM) data began several decades ago, following the production of multiple commercial flow cytometry platforms. Fluorescence standardization methods have been established since the late 1990's, yet these have not been widely adopted by the FCM community for a variety of reasons. Nonetheless, extensive literature and commercially available materials have been developed to facilitate fluorescence calibration in cellular analysis[1-7]. These protocols can be readily applied to the analysis of small particles, as demonstrated in this current study. Although it can be assumed that all commercial flow cytometers can fully resolve cellular populations from noise, the same is not true for small particles such as EVs. Therefore, supplementary methods need to be employed to validate small particle flow cytometry analysis.

The detection and characterization of small particles, in the form of viruses, using light scatter triggering was published over 40 years ago[8]. Calibration of light scatter from a flow cytometer was demonstrated for small particles in 2009 by Fattacioli *et al.,* and specifically for EVs by van der Pol *et al.* in 2012[9, 10]. Despite having been established for a decade, the use of light scatter calibration in small particle FCM has been limited, partly owing to the complexity of Mie Theory-based scatter modeling required for light scatter signal normalization. In 2015, a commercial light scatter calibration assay (Rosetta Calibration by Exometry) was released to facilitate this process and used in a flow cytometry standardization study for the International Society on Thrombosis and Haemostasis (ISTH)[11]. In 2019, FCM_{PASS}, a free alternative small particle flow cytometer calibration software package for light scatter and fluorescence became available[12]. While there is now both software and materials available for light scatter calibration, further support in the form of education and resource materials is required for the correct implementation and assessment in accuracy of calculated models.

Currently, both fluorescence and light scatter calibration is under-utilized in the field of small particle FCM. The utilization of calibration for small particle analysis is, however, critical due to the majority of commercial FCM instrumentation working at their detection limits when analyzing EVs and other biological particles <200 nm in diameter. Since flow cytometers have a wide range of optical configurations, methods are required for standardized data reporting such that meaningful biological conclusions can be made. There is currently no

consensus method for this. Here, we combine scatter and fluorescence calibration, using currently available methods and reference materials such that data can be converted to standard units for direct comparison between two different flow cytometry platforms. We show that the calibrations performed using FCM_{PASS} software package can be validated using a biological reference particle[12].

Materials and Methods

Sample preparation. MV-M-sfGFP (ViroFlow Technologies, Canada) was re-constituted as per manufacturer's instructions. The concentration of virus particles was adjusted to $5x10^8$ particles mL^{-1} according to the concentration provided by the manufacturer and labeled with anti-GFP PE antibody (Clone FM264G, BioLegend) at 0.4 µg mL^{-1} for a minimum of 30 minutes at room temperature, protected from light. Antibody labeled virus was diluted to ~$1x10^6$ particles mL^{-1} immediately prior to analysis by flow cytometry. Antibody alone and unstained virus samples were similarly prepared. All dilutions were made using 0.1 µm filtered PBS (PBS 1x, no Ca^{2+}, no Mg^{2+}, Wisent).

Cytometer Configuration. BD LSR Fortessa 50 mW 488 nm laser, 50 mW 561 nm, 488/10 (SSC), 561-586/15 (PE), 488-530/30 (GFP). Beckman Coulter CytoFLEX S, 80 mW 405 nm, 50 mW 561 nm, 405/8 (SSC), 561-585/42 (PE), 488-525/40 (GFP).

Small particle sample acquisition. Identical bead and antibody labeled virus samples were acquired on the LSR Fortessa (BD Biosciences, USA) and CytoFLEX S (Beckman Coulter, USA). Detector settings 1, 2 and 3 for fluorescence detection on the LSR Fortessa were determined using the PE MESF beads (QuantiBrite, BD Biosciences, USA). Setting 1 being the lowest voltage where the dimmest bead population was resolved from background and setting 3 being the highest voltage where the brightest bead population was within maximum detection limit. Setting 2 was approximately halfway between setting 1 and 3. Gain settings for fluorescence detection on the CytoFLEX S were similarly determined. For scatter calibration three separate gains were used on the CytoFLEX S. For setting 1, side scatter (SSC) gain was chosen where the 600 nm NIST-traceable polystyrene bead population was within the range of detection. Setting 2 and setting 3 SSC voltages were the same for all three settings acquired on the LSR Fortessa since it was not possible to use multiple voltages to collect meaningful data. The difference between the three scatter data sets on the LSR Fortessa are based on gating of MV-M-sfGFP which changed due to PE voltage settings. All samples were acquired on the lowest preset instrument flow rates for one minute. For the CytoFLEX S this was 10 µL min-1, verified using the built in calibration software and weighing samples of deionized water before and after acquisition. For the LSR Fortessa the flow rate was approximately 20 µL min^{-1}.

Cytometer calibration. Light scatter calibration was performed using 81, 100, 152, 203, 269, 303, 345, 401, 453, 568, 600 nm polystyrene NIST-traceable beads (ThermoFisher Scientific, USA) and 480 and 730 nm silica NIST-traceable beads (ThermoFisher Scientific, USA). Median SSC intensity (488 nm SSC on LSR Fortessa, 405 nm SSC on CytoFLEX S) were gated using FlowJo (v10.5.3, USA). Mie modeling and subsequent conversion of light scatter intensity to diameter was performed using FCM_{PASS} software (http://nanopass.ccr.cancer.gov)[12]. Model input settings including refractive indices, bead information, and statistics can be found in **Supplementary Information 1** and **2**, with model outputs shown in **Supplementary Figure 1** and **2**. The collection half-angle refers to the angle of light being collected around the particle within the sheath of the instrument. Fluorescence calibration was performed using PE MESF beads (QuantiBrite PE, Cat# 340495, Lot 73318, BD Biosciences, USA) at a voltage/gain that allowed for the brightest bead to be within the range of detection of the instrument. Median PE was gated using FlowJo. Fluorescence calibration was performed using FCM_{PASS} software. These PE MESF values were used to cross-calibrated 8-peak rainbow bead (Cat# RCP-30-5A, Lot AF01, Spherotech, USA) data acquired at the same settings as the PE MESF beads. The 8-peak rainbow beads were then used to calibrate the PE intensity scales at different acquisition settings. This is a cost effective method demonstrating the cross calibration of different types of fluorescence calibration beads, where the 8-peak rainbow beads will also have more populations on-scale at the high voltage/gain settings. Virus concentration on the CytoFLEX S and LSR Fortessa was calculated using 200 nm fluorescent polystyrene spike-in beads (Green FluoSpheres, Cat# F8848, ThermoFisher Scientific,

USA) using the mean concentration of beads acquired using the CytoFLEX S after calibration of the fluidic system at a low flow rate.

Data Analysis. Fluorescence and light scatter comparison figures were created using MATLAB (R2019b, Mathworks, Inc). Samples were gated in FlowJo with representative gating strategies on the CytoFLEX S and LSR Fortessa shown in **Figure 1.** Sample controls and their comparison to gated MV-M-sfGFP can been seen for both instruments in **Supplementary Figure 3**.

Results

Fluorescence calibration. The PE intensity of anti-GFP PE labeled MV-M-sfGFP from the LSR Fortessa and CytoFLEX S ranged in arbitrary units of intensity from 110 to 17322 using three different gain/voltage settings as defined in the methods section, **Figure 2A and 2B**. Upon calibration of fluorescence intensity to PE MESF units, values ranged from just 89 to 127 PE MESF. Data irrespective of instrument or instrument settings were comparable.

Light scatter calibration. Side-scatter intensity of MV-M-sfGFP was compared across the LSR Fortessa and CytoFLEX S. Three scatter settings were tested on the CytoFLEX S and LSR Fortessa (defined in methods section). Light scatter intensity for SSC across the LSR Fortessa and CytoFLEX S ranged from 346 to 13014 arbitrary units, **Figure 2C and 2D**. Calibration of light scatter to diameter in nanometers resulted in values that ranged from just 123 to 126 nm.

Concentration calibration. Samples were measured on the CytoFLEX S and LSR Fortessa for one minute. The LSR Fortessa's technical specifications state the low flow rate to be 12 µL min^{-1}, while the CytoFLEX S's lowest flow rate is 10 µL min^{-1}. The recorded number of MV-M-sfGFP events if fully detected should theoretically have been 20% higher than those of the CytoFLEX S. In practice the mean total count difference between instruments was 39%. This indicates that either the flow rate between the two instruments is not as stated or the virus was resolved to different extents between the instruments. When spike-in beads were used normalize the MV-M-sfGFP concentration between the two instruments the calculated concentration was shown to be 30% higher on the CytoFLEX S at 1.76 x 10^6 particles mL^{-1} versus 1.34 x 10^6 particles mL^{-1} **Figure 2E and 2F**. As the MV-M-sfGFP is fully resolved on the CytoFLEX S, this suggests the LSR Fortessa was unable to fully resolve the MV-M-sfGFP. It can be seen that the MV-M-sfGFP was not completely resolvable above the LSR Fortessa SSC triggering threshold, **Figure 2A, B**, this likely accounts for some of the difference observed in concentration. This may have also influenced median statistics for diameter observed. It is notable that despite the same sample being analyzed between the instruments at difference settings and appearing to be resolvable to the same extent, the recorded concentration had a variance of 11.9% and 10% on the CytoFLEX S and LSR Fortessa, respectively. This is likely to do with the consistency of the flow rate and is something that would need to be further investigated for methods of improvement, **Supplementary Figure 4**.

Calibration overview. It can be seen that when overlaying uncalibrated MV-M-sfGFP data between the two instruments, very few comparisons can be made despite these being the same sample run between two instruments, **Figure 3A**. This is the current state of much of the literature. Upon calibrating the MV-M-sfGFP data on both instruments to units of PE MESF units, it can be seen that the PE staining data overlaps and is fully concordant between instruments. While the use the light scatter calibration is a valid method of reporting light scatter measurements it by definition describes the statistical quantity of light that will reach the detector which is influenced by the collection angle of the instrument. If the same population is acquired on two instruments, one with a large collection angle and one with a smaller collection angle, the scattering cross section of the population will be higher on the instrument with the larger collection angle. This is observed with the CytoFLEX S and LSR Fortessa data. The scattering cross-section of the virus on the CytoFLEX S, which had a predicted collection half angle of 53.2° was 1953 nm^2, while the LSR Fortessa with a predicted collection half-angle of 46.1° had a scattering cross-section of 994 nm^2, **Figure 3B**. In order to normalize light scatter data irrespective of collection angle, diameter must be used. It can be seen that when the MV-M-sfGFP data is normalized to units of diameter in nanometers the data between the instruments becomes fully concordant, **Figure 3C**.

Discussion

Two main factors contributed to the consistency of the results in this report. 1) The same validation sample, PE-labeled MV-M-sfGFP, was used for all of the data acquisition. This eliminated inconsistencies in staining intensity and highlight the importance of accurate reporting of both antibody concentrations as well as particle concentrations used for antibody labeling experiments in small particle FCM. Discrepancies in either of these parameters greater than a factor of two can significantly impact staining intensity of small particles[13]. 2) The specific types of beads used to perform the calibrations were pivotal for this standardization process. For the light scatter calibration beads, it was important that they were accurately sized with known refractive indices, and non-fluorescent, as fluorophores would absorb light and therefore affect subsequent scatter. Light scatter calibration should be performed accordingly on samples acquired by SSC-trigger threshold. This allowed for confident determination of the limit of light scatter sensitivity. For fluorescence calibration, MESF beads with matching fluorophore to the biological particle were used. This was essential for the fluorescence intensities to be comparable between instruments with differing optical configurations, such as filter sets and laser wavelengths for excitation[13]. In summary, the methods employed here compellingly show that standardized data reporting of fluorescence and light scatter is achievable for small particle FCM data when it is converted to standard units of MESF and diameter.

MV-M-sfGFP was used as a proof-of-principle sample due to it being a well-defined, homogeneous population. Validation of these methodologies for the extracellular vesicle (EV) field are required but will be more challenging due to the majority of EVs likely being below the triggering threshold and having a Power-law distribution. This will mean that normalization of the light scatter and fluorescence data between instruments will heavily rely upon accurate quantitation of the concentration. This will be challenging as relatively large variations can occur in concentration with identical samples on the same platform, as we have shown in this pilot study. Further testing of fluidic stability and acquisition time for their effect on recorded concentration variation with an easily detectable, homogeneous population should therefore be a priority for laboratories attempting to use concentration measurements and would be the next step in this line of work.

Ultimately, calibration is critical to allow for meaningful biological conclusions and allow reproduction of work. The use of calibration will also aid researchers in identifying optimal assays and equipment for their work. While literature is beginning to emerge that has utilized fluorescence, to-date small particle standardization studies have predominantly utilized light scatter normalization methods[11, 14-17]. While light scatter calibration has great utility, fluorescence calibration should be seen as a priority in any study utilizing fluorescence staining, whether it is immunophenotyping or simply using a bulk stain. This is due to the majority of studies not reporting total detected counts of all events, but generally the count of a fluorescent event. To this end, a follow up standardization study is required that utilizes both fluorescence and light scatter calibration to compare instrument sensitivities and further validate the findings of this pilot study.

While the need for calibration is essential for the field to progress, its use alone does not ensure quality of research. The use of optimal experimental design with controls such as serial dilution to ensure single particle detection, buffer with reagent controls to shown lack of artefacts, and isotype or negative staining controls to show specificity are all required. The consensus for reporting of the methods and experimental design will likely need to be reached for researchers to make easy comparisons between work and allow for reproduction of data. These important components are currently being addressed by the International Society of Extracellular Vesicles, International Society for Advancement of Cytometry, and International Society for Thrombosis and Haemostasis flow cytometry working group.

Funding acknowledgements

JAW is supported by U.S. National Institutes of Health, National Cancer Institute Grant Number: 1ZIA-BC011502.

Declaration of interest statement

JAW has patents and patent applications related to EV analysis and is a 2019-2023 ISAC Marylou Ingram Scholar. VAT is CSO of ViroFlow Technologies and is a 2018-2022 ISAC SRL Emerging Leader.

References

1. Wood, J. C., Fundamental flow cytometer properties governing sensitivity and resolution. *Cytometry* **1998,** *33* (2), 260-6.
2. Wood, J. C.; Hoffman, R. A., Evaluating fluorescence sensitivity on flow cytometers: an overview. *Cytometry* **1998,** *33* (2), 256-9.
3. Hoffman, R. A., Standardization, calibration, and control in flow cytometry. *Curr Protoc Cytom* **2005,** *Chapter 1*, Unit 1 3.
4. Wang, L.; Hoffman, R. A., Standardization, Calibration, and Control in Flow Cytometry. *Curr Protoc Cytom* **2017,** *79*, 1 3 1-1 3 27.
5. Gaigalas, A. K.; Wang, L.; Schwartz, A.; Marti, G. E.; Vogt, R. F., Jr., Quantitating Fluorescence Intensity From Fluorophore: Assignment of MESF Values. *J Res Natl Inst Stand Technol* **2005,** *110* (2), 101-14.
6. Schwartz, A.; Gaigalas, A. K.; Wang, L.; Marti, G. E.; Vogt, R. F.; Fernandez-Repollet, E., Formalization of the MESF unit of fluorescence intensity. *Cytometry B Clin Cytom* **2004,** *57* (1), 1-6.
7. Schwartz, A.; Wang, L.; Early, E.; Gaigalas, A.; Zhang, Y. Z.; Marti, G. E.; Vogt, R. F., Quantitating Fluorescence Intensity from Fluorophore: The Definition of MESF Assignment. *J Res Natl Inst Stand Technol* **2002,** *107* (1), 83-91.
8. Hercher, M.; Mueller, W.; Shapiro, H. M., Detection and discrimination of individual viruses by flow cytometry. *J Histochem Cytochem* **1979,** *27* (1), 350-2.
9. Fattaccioli, J.; Baudry, J.; Emerard, J. D.; Bertrand, E.; Goubault, C.; Henry, N.; Bibette, J., Size and fluorescence measurements of individual droplets by flow cytometry. *Soft Matter* **2009,** *5* (11), 2232-2238.
10. van der Pol, E.; van Gemert, M. J.; Sturk, A.; Nieuwland, R.; van Leeuwen, T. G., Single vs. swarm detection of microparticles and exosomes by flow cytometry. *J Thromb Haemost* **2012,** *10* (5), 919-30.
11. van der Pol, E.; Sturk, A.; van Leeuwen, T.; Nieuwland, R.; Coumans, F.; group, I.-S.-V. W., Standardization of extracellular vesicle measurements by flow cytometry through vesicle diameter approximation. *J Thromb Haemost* **2018,** *16* (6), 1236-1245.
12. Welsh, J. A.; Horak, P.; Wilkinson, J. S.; Ford, V. J.; Jones, J. C.; Smith, D.; Holloway, J. A.; Englyst, N. A., FCMPASS Software Aids Extracellular Vesicle Light Scatter Standardization. *Cytometry Part A* **2019**.
13. Tang, V. A.; Fritzsche, A. K.; Renner, T. M.; Burger, D.; Lannigan, J. A.; Brittain, G. C.; Ouellet, C. V.; van der Pol, E.; Langlois, M.-A., Engineered Retroviruses as Fluorescent Biological Reference Particles for Nanoscale Flow Cytometry. *bioRxiv* **2019**, 614461.
14. Morales-Kastresana, A.; Musich, T. A.; Welsh, J. A.; Telford, W.; Demberg, T.; Wood, J. C. S.; Bigos, M.; Ross, C. D.; Kachynski, A.; Dean, A.; Feton, E. J.; Van Dyke, J.; Tigges, J.; Toxavidis, V.; Parks, D. R.; Overton, W. R.; Kesarwala, A. H.; Freeman, G. J.; Rosner, A.; Perfetto, S. P.; Pasquet, L.; Terabe, M.; McKinnon, K.; Kapoor, V.; Trepel, J. B.; Puri, A.; Kobayashi, H.; Yung, B.; Chen, X. Y.; Guion, P.; Choyke, P.; Knox, S. J.; Ghiran, I.; Robert-Guroff, M.; Berzofsky, J. A.; Jones, J. C., High-fidelity detection and sorting of nanoscale vesicles in viral disease and cancer. *Journal of Extracellular Vesicles* **2019,** *8* (1).
15. Stoner, S. A.; Duggan, E.; Condello, D.; Guerrero, A.; Turk, J. R.; Narayanan, P. K.; Nolan, J. P., High sensitivity flow cytometry of membrane vesicles. *Cytometry A* **2016,** *89* (2), 196-206.
16. Görgens, A.; Bremer, M.; Ferrer-Tur, R.; Murke, F.; Tertel, T.; Horn, P. A.; Thalmann, S.; Welsh, J. A.; Probst, C.; Guerin, C.; Boulanger, C. M.; Jones, J. C.; Hanenberg, H.; Erdbrügger, U.; Lannigan, J.; Ricklefs, F. L.; El Andaloussi, S.; Giebel, B., Optimisation of Imaging Flow Cytometry for the Analysis of Single Extracellular Vesicles by Using Fluorescence-tagged Vesicles as Biological Reference Material. *Journal of Extracellular Vesicles* **2019**.
17. Lacroix, R.; Robert, S.; Poncelet, P.; Kasthuri, R. S.; Key, N. S.; Dignat-George, F.; Workshop, I. S., Standardization of platelet-derived microparticle enumeration by flow cytometry with calibrated beads: results of the International Society on Thrombosis and Haemostasis SSC Collaborative workshop. *J Thromb Haemost* **2010,** *8* (11), 2571-4.

Figure 1 - Representative gating strategy used between flow cytometers. The side scatter versus GFP fluorescence of MV-M-sfGFP are shown on the CytoFLEX S (A) and LSR Fortessa (B). The gating of MV-M-sfGFP on GFP intensity versus anti-GFP-PE staining are shown for the CytoFLEX S (C) and LSR Fortessa (D). Background reference noise, MV-M-sfGFP, and spike-in beads are annotated in (A).

Figure 2 - Comparison of uncalibrated vs. calibrated parameters. Uncalibrated SSC-H intensity (A) and calibrated diameter (B). Median SSC and diameter statistics are shown below each population and are represented by the horizontal line through the scatter plot. Comparison of uncalibrated PE intensity (C) and calibrated PE MESF intensity (D). Median PE intensity and PE MESF statistics are shown below each population and are represented by the horizontal line through the scatter plot. Comparison of uncalibrated concentration (E) and calibrated concentration (F).

Figure 3 - Representative overlay of uncalibrated versus calibrated parameters. The gated virus of Set 2 for the CytoFLEX S (black) and LSR Fortessa (Red) are overlaid in plots A, B, C. With plot A showing uncalibrated data, plot B showing PE MESF calibrated and scatter Cross-Section (CS) calibrated data. Plot C shows PE MESF calibrated and diameter calibrated data.

Supplementary Figure 1 - Light scatter modelling outputs of CytoFLEX S. The model fit (A) depicts the predicted versus acquire scatter for each bead. The predicted collection angle (B) shows the collection angle used to create the scatter-diameter model (C).

Supplementary Figure 2 - Light scatter modelling outputs of LSR Fortessa. The model fit (A) depicts the predicted versus acquire scatter for each bead. The predicted collection angle (B) shows the collection angle used to create the scatter-diameter model (C).

Supplementary Figure 3 - Sample controls. The PBS controls for the CytoFLEX S (A, D) and LSR Fortessa (H, K) are shown alongside the noGFP expressing virus (B, E, I, L) and the GFP expressing virus (C, F, J, M).

Supplementary Figure 4 - Sampling rate of gated GFP-expressing virus on the CytoFLEX S (A) and LSR Fortessa (B).

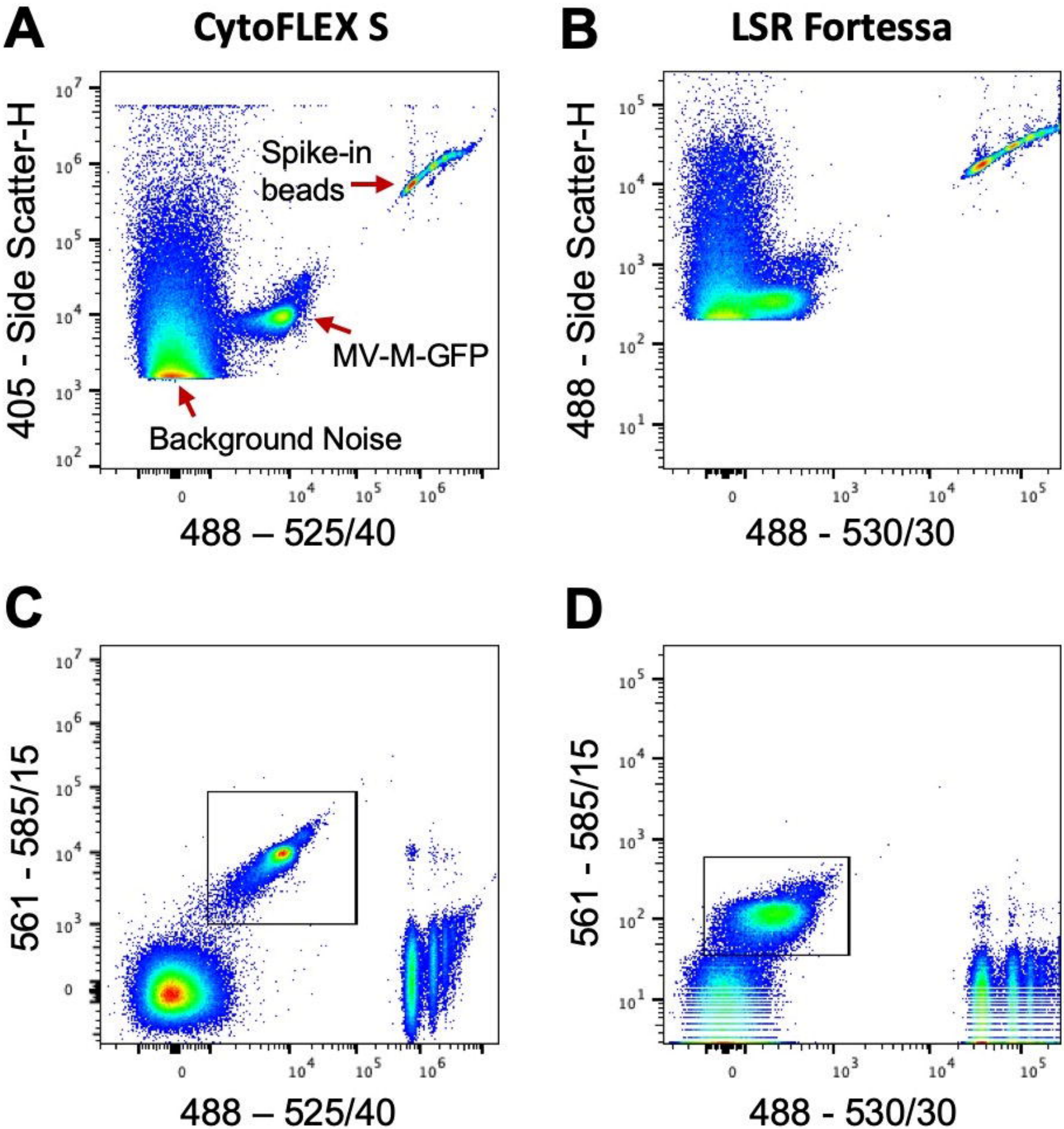
A
CytoFLEX S
405 - Side Scatter-H
Spike-in beads
MV-M-GFP
Background Noise
488 – 525/40
B
LSR Fortessa
488 - Side Scatter-H
488 - 530/30
C
561 - 585/15
488 – 525/40
D
561 - 585/15
488 - 530/30

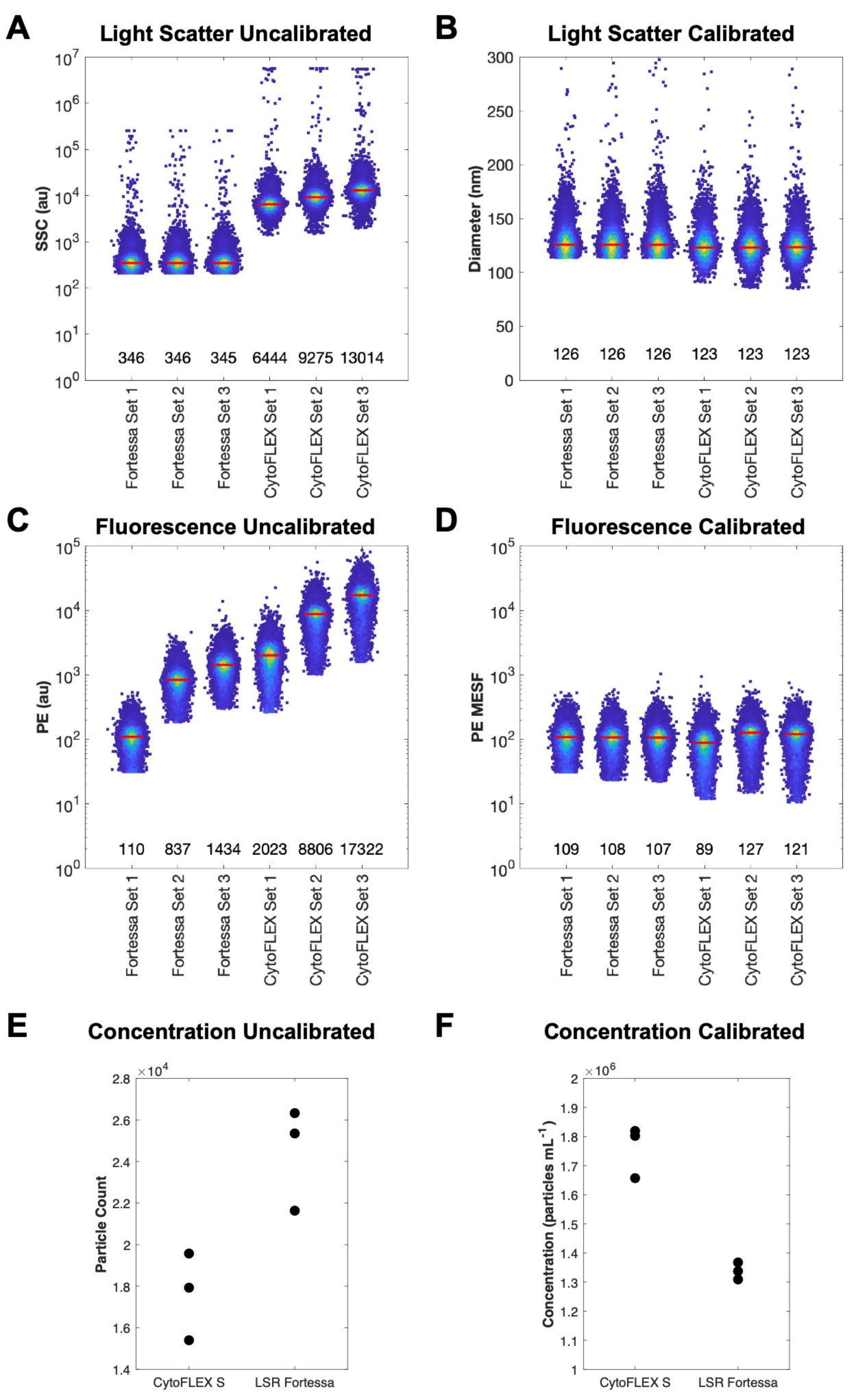
A
Light Scatter Uncalibrated
SSC (au)
346 346 345 6444 9275 13014
B
Light Scatter Calibrated
Diameter (nm)
126 126 126 123 123 123
C
Fluorescence Uncalibrated
PE (au)
110 837 1434 2023 8806 17322
D
Fluorescence Calibrated
PE MESF
109 108 107 89 127 121
Fortessa Set 1
Fortessa Set 2
Fortessa Set 3
CytoFLEX Set 1
CytoFLEX Set 2
CytoFLEX Set 3
E
Concentration Uncalibrated
Particle Count
CytoFLEX S
LSR Fortessa
F
Concentration Calibrated
Concentration (particles mL-1)
CytoFLEX S
LSR Fortessa

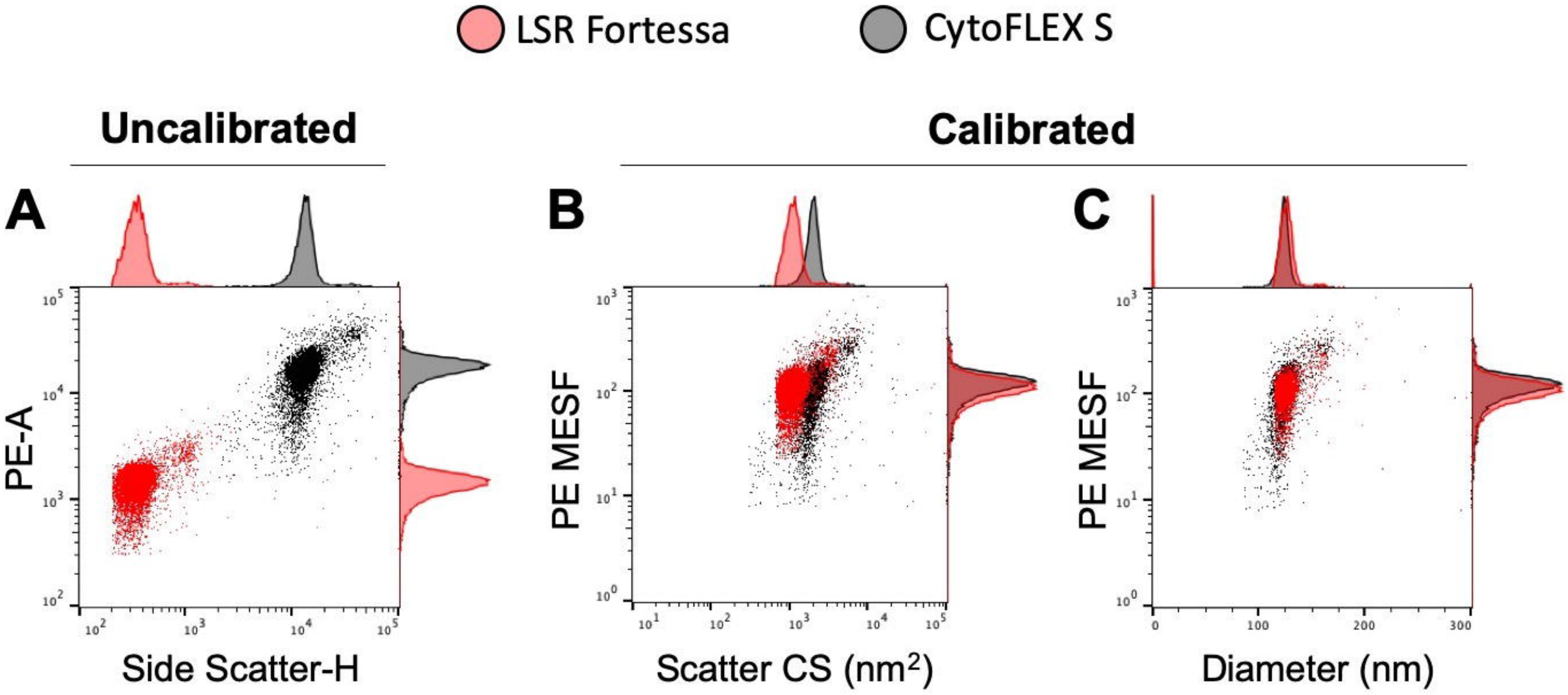
LSR Fortessa
CytoFLEX S
Uncalibrated
Calibrated
A
B
C
PE-A
Side Scatter-H
PE MESF
Scatter CS (nm²)
PE MESF
Diameter (nm)

CytoFLEX S

A

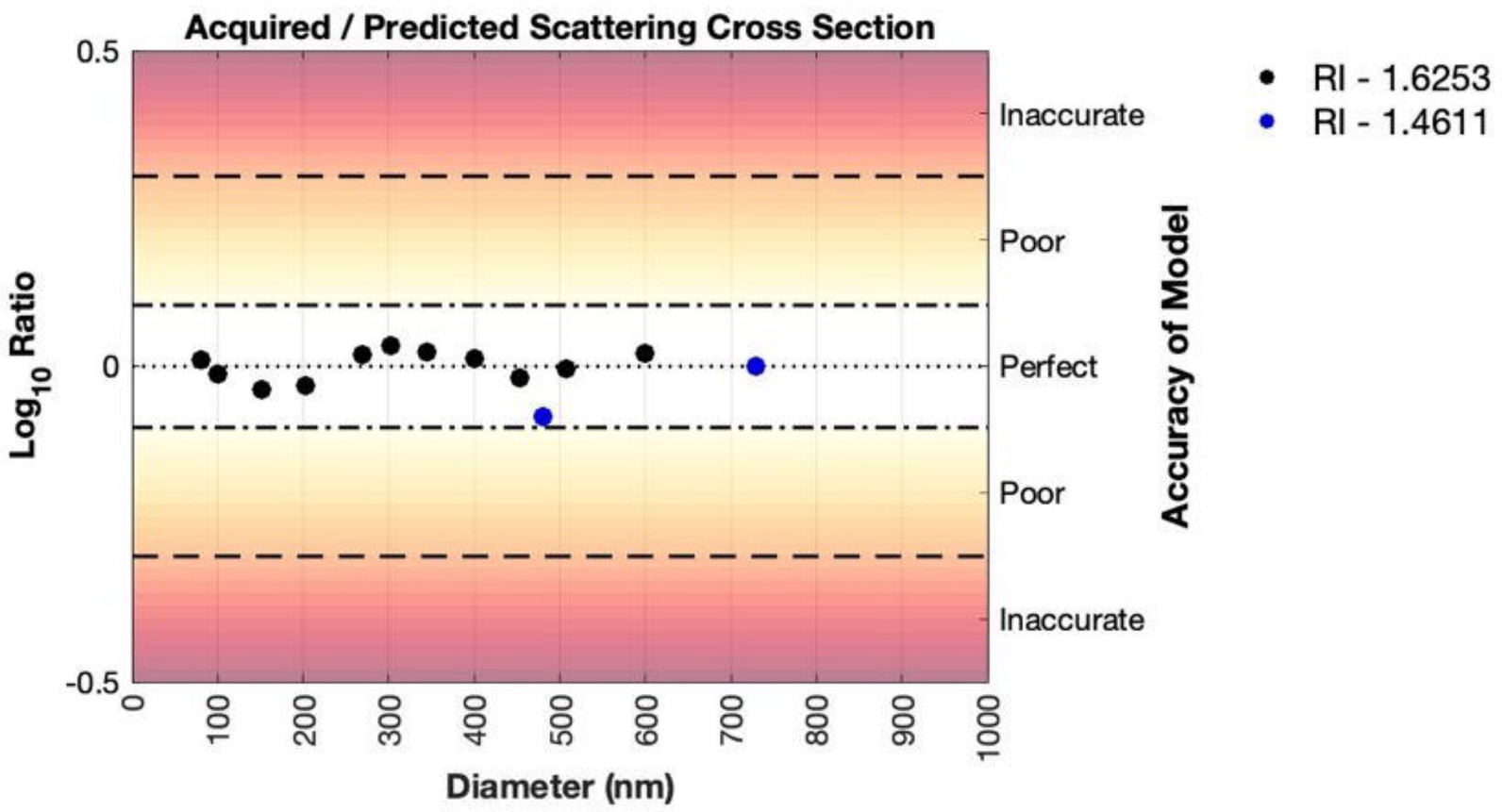

B

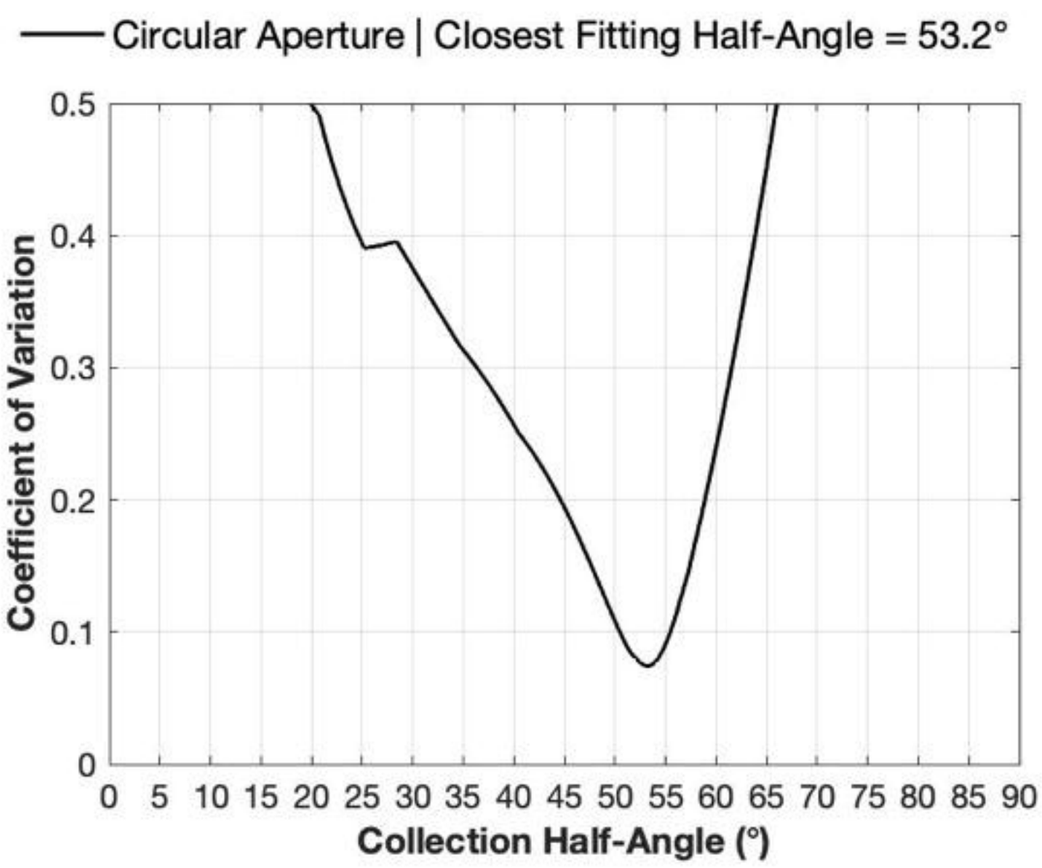

C

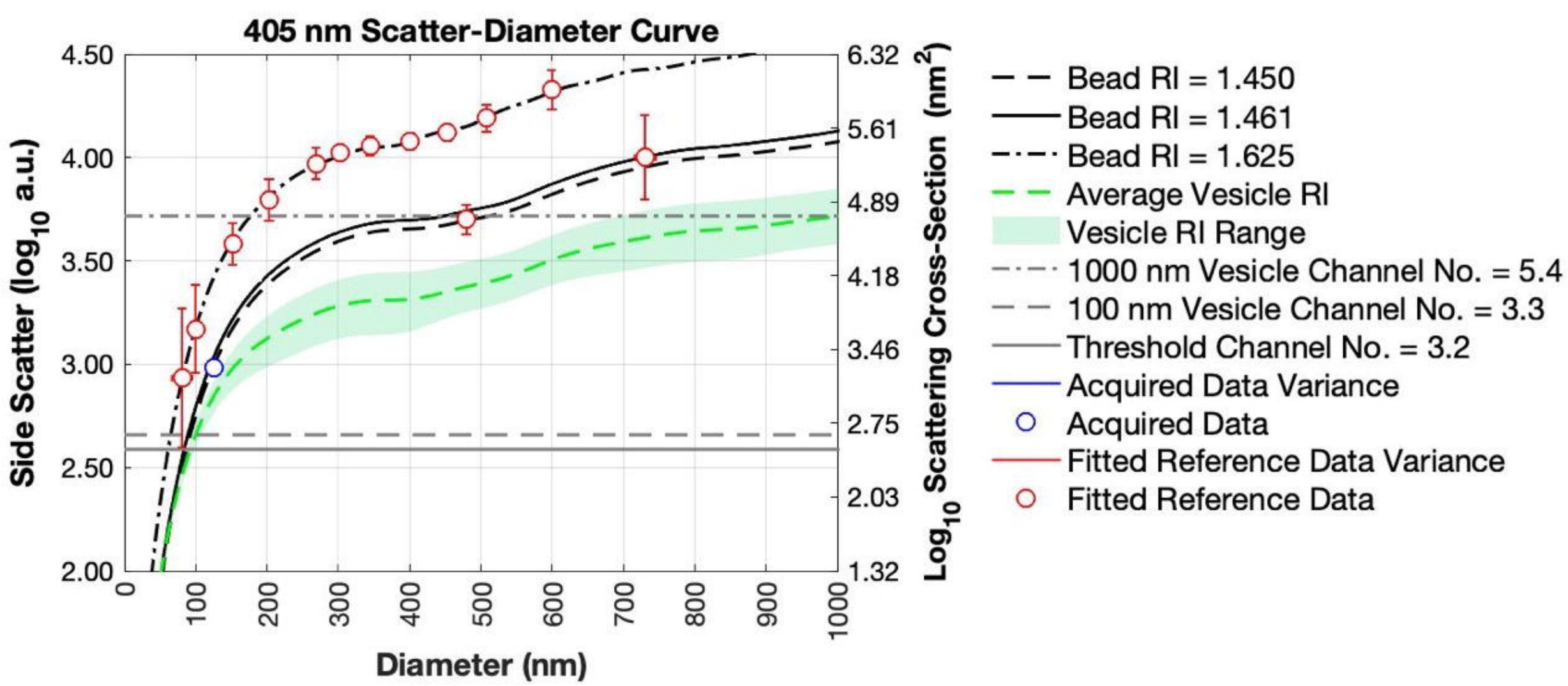

LSR Fortessa

A

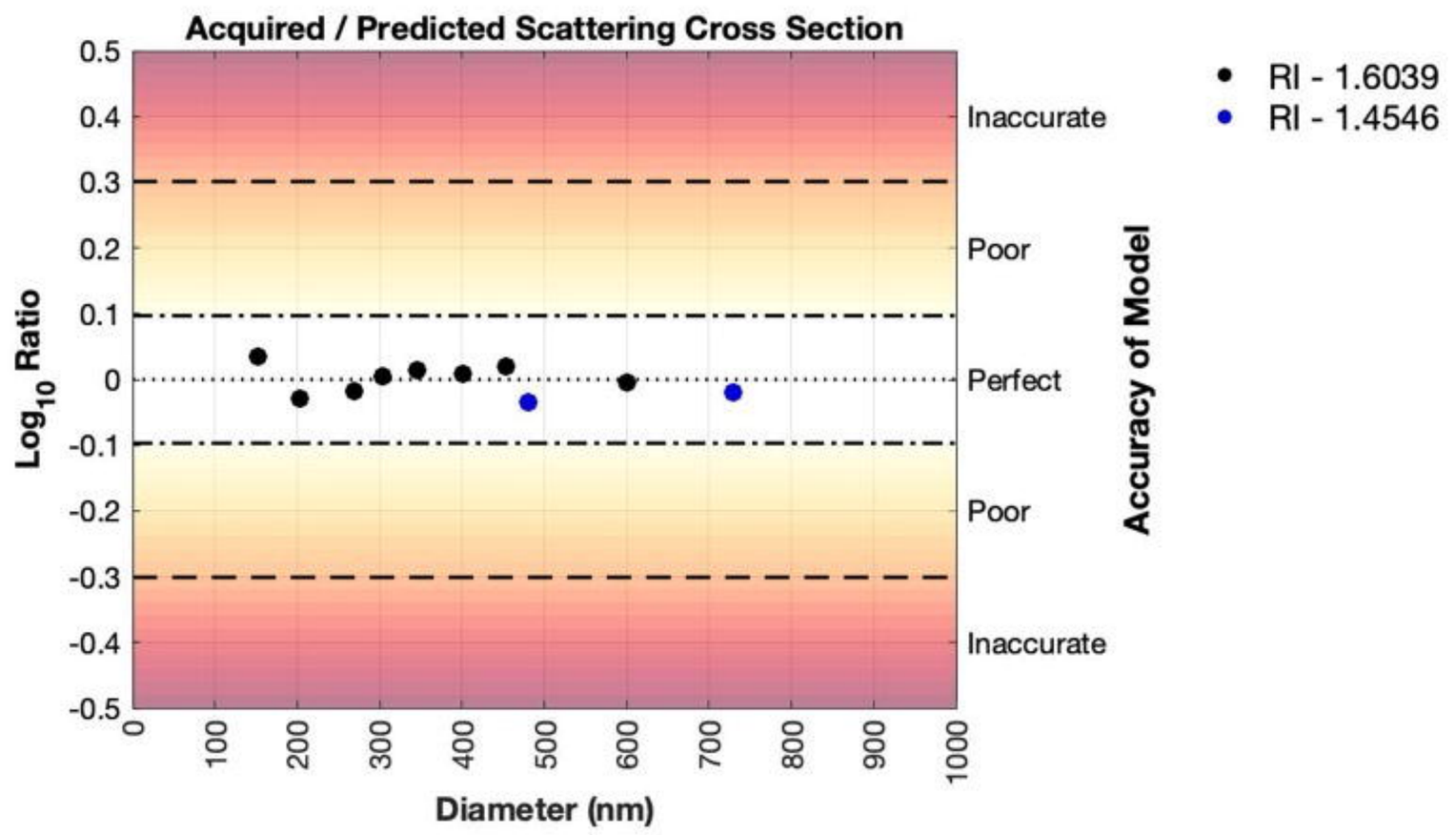

B

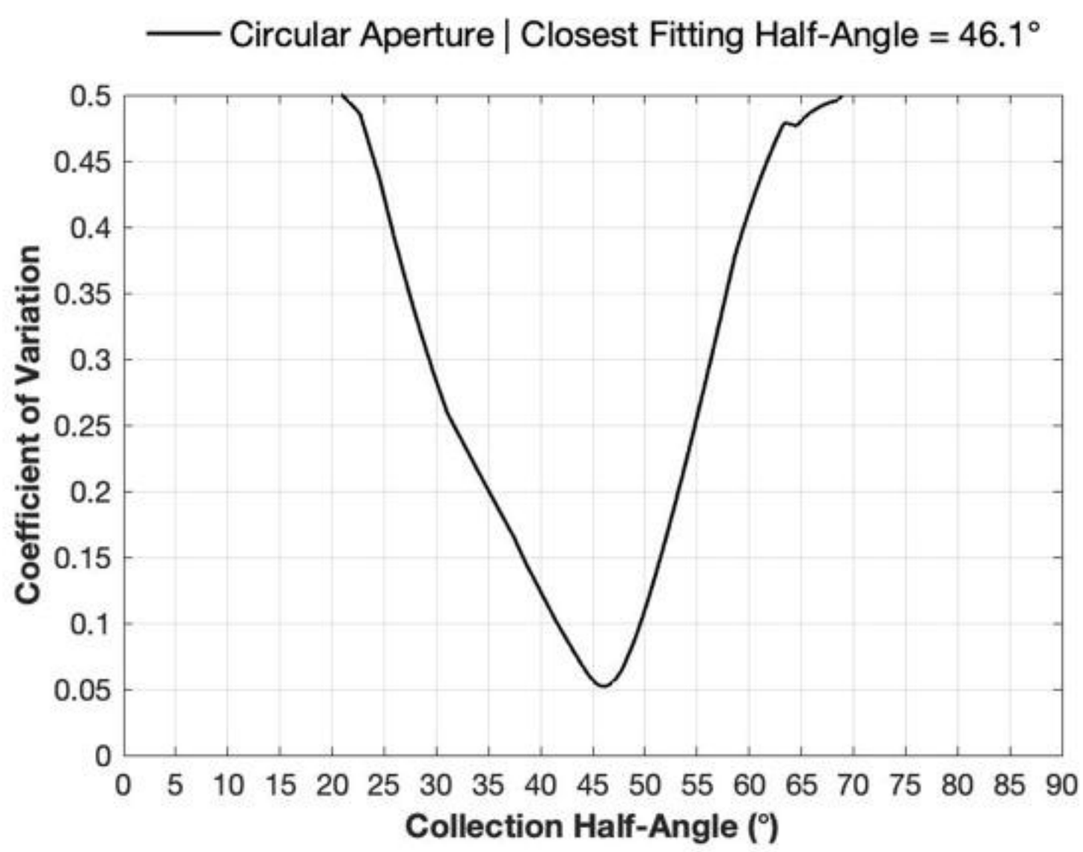

C

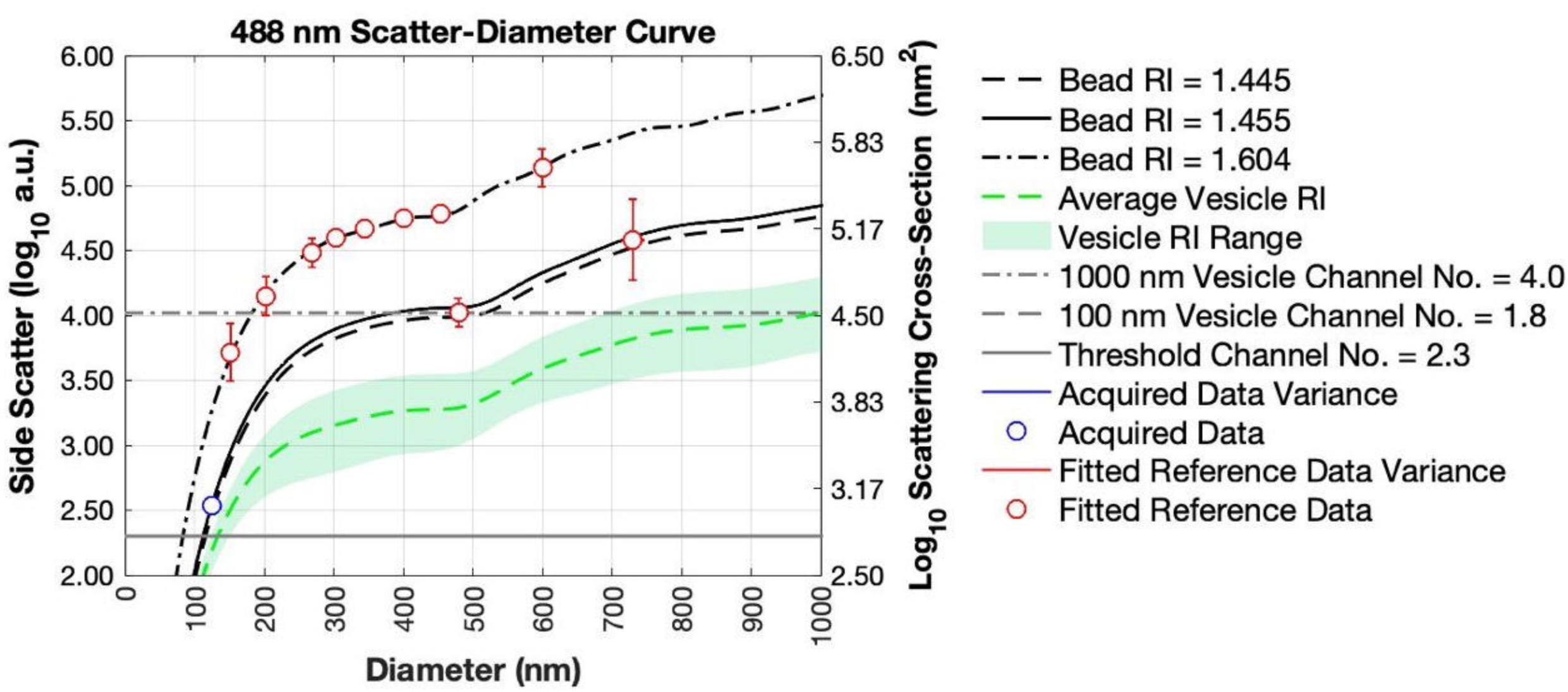

CytoFLEX S

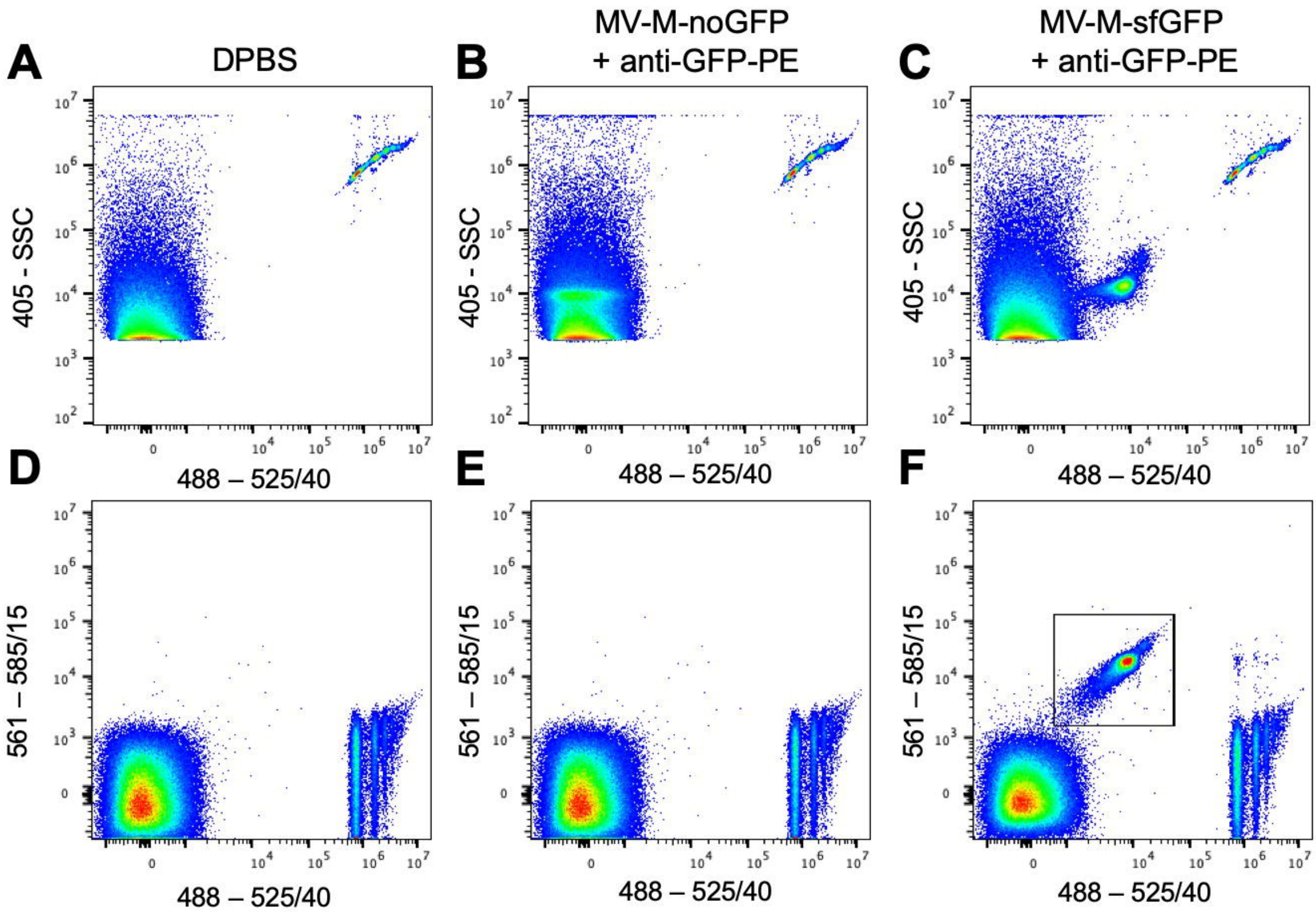

LSR Fortessa

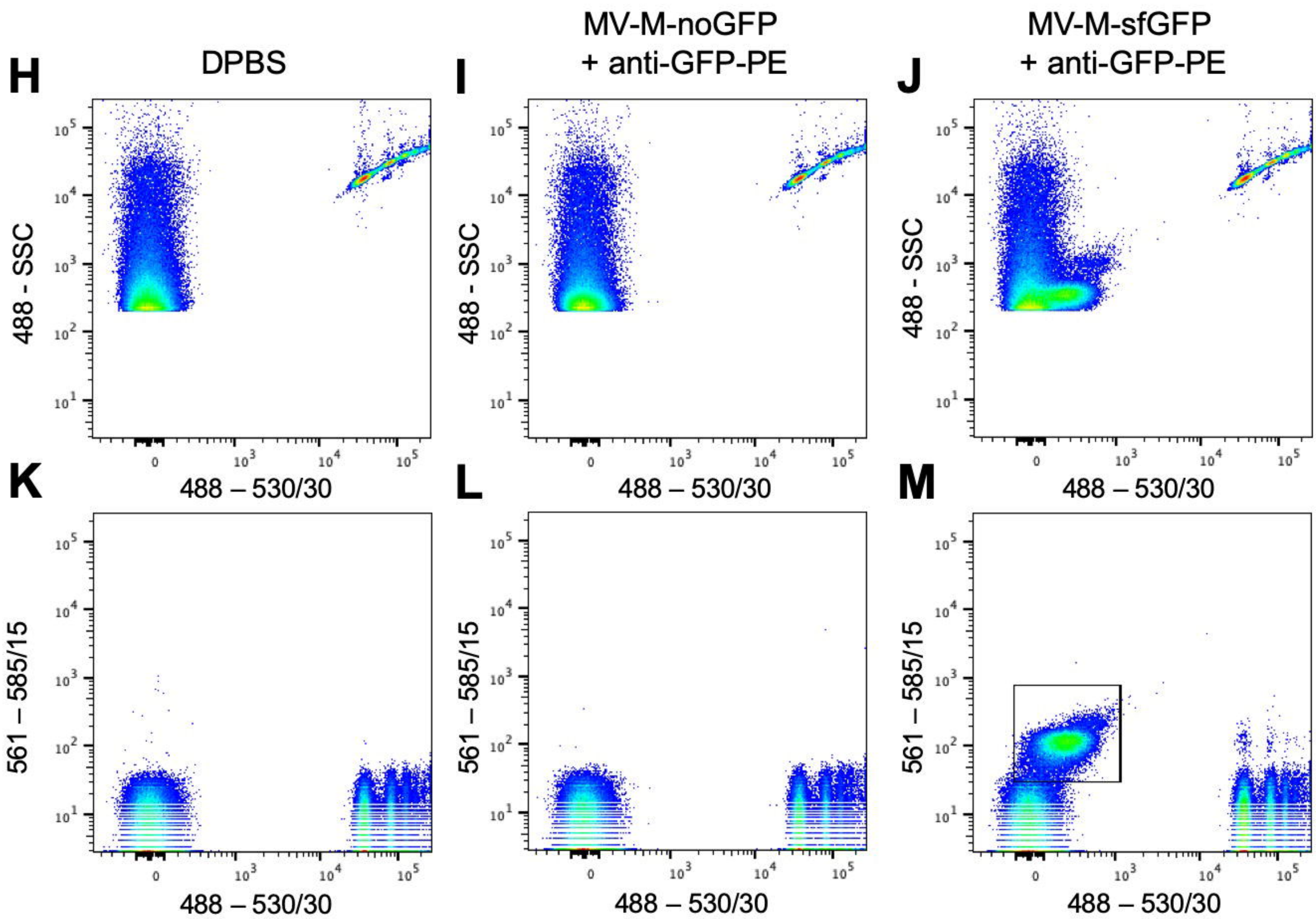

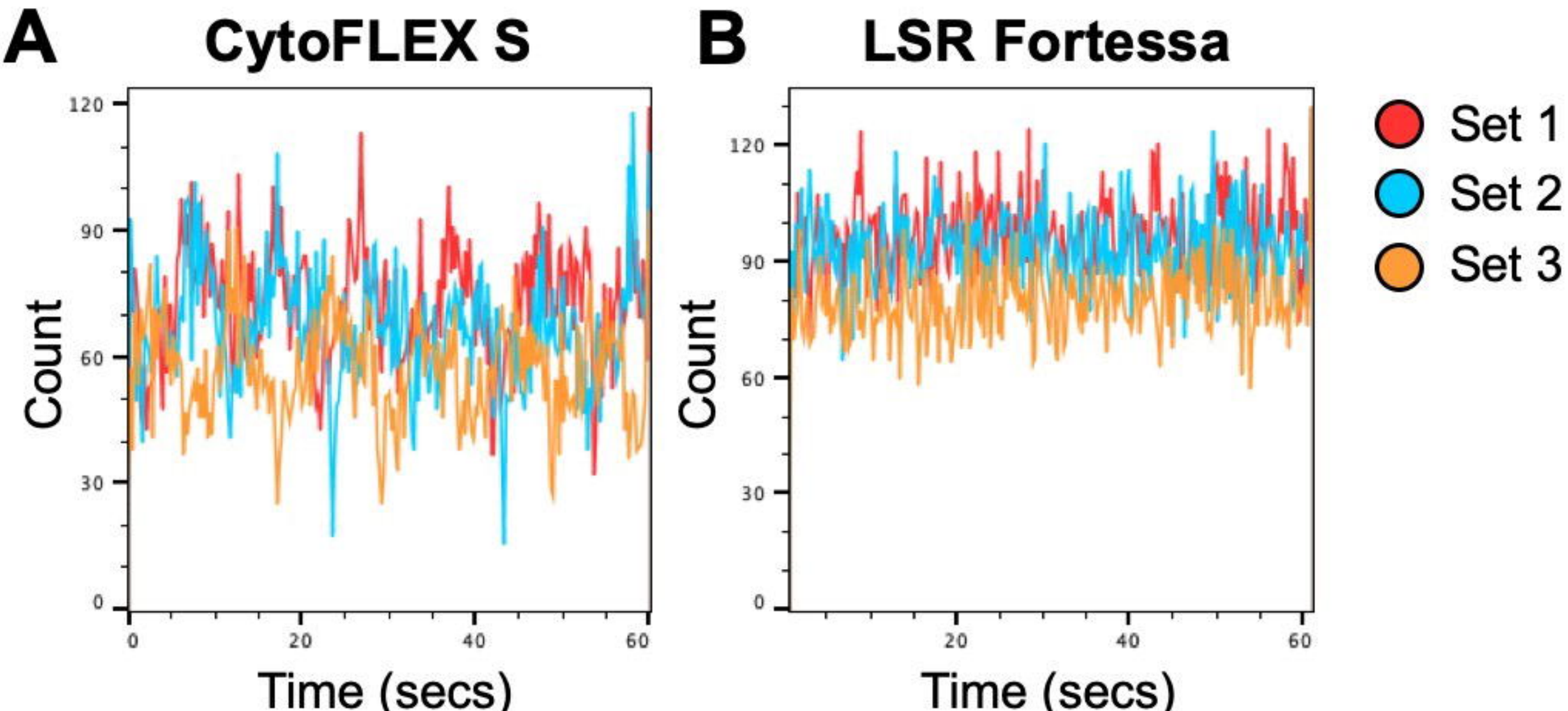
A
CytoFLEX S
B
LSR Fortessa
Count
Time (secs)
0
30
60
90
120
0
20
40
60
Set 1
Set 2
Set 3